Reference to published article:
Robertson, J.M., Nesbitt, J.A. & Lindsay, M.B.J. (2019). Aqueous- and solid-phase molybdenum geochemistry of oil sands fluid petroleum coke deposits, Alberta, Canada. *Chemosphere (Oxford),* 217: 715–723. https://doi.org/10.1016/j.chemosphere.2018.11.064

Aqueous- and solid-phase molybdenum geochemistry of oil sands fluid petroleum coke deposits, Alberta, Canada

Jared M. Robertson, Jake A. Nesbitt, Matthew B.J. Lindsay*

Department of Geological Sciences, University of Saskatchewan, Saskatoon, SK, S7N 5E2, Canada

* Corresponding author: 114 Science Place, Department of Geological Sciences, University of Saskatchewan, Saskatoon, SK, S7N 5E2, Canada; Tel: +1 306 966 5693

Email address: matt.lindsay@usask.ca (M.B.J. Lindsay)

Keywords: oil sands; petroleum coke; molybdenum; water; geochemistry; X-ray absorption spectroscopy

Abstract

Fluid petroleum coke generated at oil sands operations in the Athabasca Oil Sands Region of northern Alberta, Canada, contains elevated concentrations of molybdenum (Mo) and other metals including nickel (Ni) and vanadium (V). Solid-phase Mo concentrations in fluid petroleum coke are typically 10 to 100 times lower than V and Ni, yet dissolved Mo concentrations in associated pore waters are often comparable with these metals. We collected pore water and solids from fluid petroleum coke deposits in the AOSR to examine geochemical controls on Mo mobility. Dissolved Mo concentrations increased with depth below the water table, reaching maxima of 1.4 to 2.2 mg L^{-1}, within a mixing zone between slightly acidic and oxic meteoric water and mildly alkaline and anoxic oil sands process-affected water (OSPW). Dissolved Mo concentrations decreased slightly with depth below the mixing zone. X-ray absorption spectroscopy revealed that Mo(VI) and Mo(IV) species were present in coke solids. The Mo(VI) occurred as tetrahedrally coordinated MoO_4^{2-} adsorbed via inner- and outer-sphere complexation, and was coordinated in an environment similar to Fe-(hydr)oxide surface complexes. The OSPW likely promoted desorption of outer-sphere Mo(VI) complexes, resulting in higher dissolved Mo concentrations in the mixing zone. The principal Mo(IV) species was MoS_2, which originated as a catalyst added upstream of the fluid coking process. Although MoS_2 is likely stable under anoxic conditions below the mixing zone, oxidative weathering in the presence of meteoric water may promote long-term Mo release.

1. Introduction

Approximately 730M tonnes of bituminous ore were mined in 2017 from the Athabasca oil sands region (AOSR) of northern Alberta, Canada. Upgraders in the AOSR convert the bitumen to synthetic crude oil and. In 2017, these upgraders produced approximately 60M m^3 of synthetic crude oil and 10.1M tonnes of petroleum coke (coke) (AER, 2018). Coking involves thermal cracking of long-chain hydrocarbons in the non-distillable bitumen fraction to volatile short-chain hydrocarbons. Although coke generated during this upgrading step can be used to fuel on-site burners, production outpaces consumption and the stockpiled inventory reached 113M tonnes by the end of 2017 (AER, 2018). Upgraders in the AOSR utilize either fluid coking or delayed coking, which generate fluid coke and delayed coke, respectively. These two types of coke exhibit different physical and chemical properties (Kessler and Hendry, 2006).

Fluid coke is a carbonaceous material enriched in sulfur and metals (e.g., Mo, V, Ni) present in the bitumen ore (Nesbitt et al., 2017; Zubot et al., 2012). This low-density material occurs as spherical grains ranging from approximately 0.05 to 50 mm in diameter (Nesbitt et al., 2017). Elevated metal concentrations in fluid coke leachates are a potential risk to water quality in the AOSR (Nesbitt et al., 2018; Nesbitt and Lindsay, 2017; Zubot et al., 2012). These leachates are acutely toxic to some aquatic organisms (Puttaswamy et al., 2010; Puttaswamy and Liber, 2011). Plants grown on fluid coke-bearing soils can accumulate Mo at concentrations known to cause molybdenosis in ruminants (Nakata et al., 2011). Molybdenum and other metals derived from airborne petroleum coke dust have also been detected in moss in the AOSR (Zhang et al., 2016). Uncovered coke stockpiles near waterways and urban communities in the United States enable the spread of coke in the form of fugitive dust (Caruso et al., 2015; Zhang et al., 2016). Due

to the ecological risks presented by coke and associated leachates, understanding the metal geochemistry of coke is critically important.

Several recent studies have examined geochemical and toxicological aspects of V, Ni and organic contaminants (i.e., naphthenic acids, polycyclic aromatic hydrocarbons) in the context of coke deposits, mine reclamation and regional contamination (Baker et al., 2012; Nesbitt et al., 2017; Nesbitt and Lindsay, 2017; Nesbitt et al., 2018; Pourrezaei et al., 2014; Puttaswamy et al., 2010; Puttaswamy and Liber, 2012, 2011; Zhang et al., 2016). Although some information on Mo within coke and associated leachates is available (Kessler and Hendry, 2006; Puttaswamy and Liber, 2012; Zubot et al., 2012), a rigorous study of Mo geochemistry of coke deposits is lacking. While solid-phase Mo concentrations (~20 mg kg^{-1}) in coke are relatively low compared to V (~1000 mg kg^{-1}) and Ni (200 mg kg^{-1}), coke pore waters contain comparable V and Mo concentrations (1 to 3 mg L^{-1}), demonstrating the large degree of Mo leachability relative to other elements in the coke (Nesbitt, 2016; Puttaswamy and Liber, 2012). These Mo concentrations are approximately three orders of magnitude greater than the average Mo concentration in the nearby Athabasca River (Shotyk et al., 2017); however, slightly elevated dissolved concentrations have been reported in the Athabasca River downstream of mines and upgraders and in oil sands process-affected water (OSPW) (Jasechko et al., 2011; Shotyk et al., 2017). In addition, the World Health Organization suggests a health-based value of 70 μg L^{-1} for Mo in drinking water (WHO, 2011), which is exceeded in coke leachates.

Molybdenum mobility is dependent on its speciation and the surrounding geochemical environment. In oxic waters at pH above 7, Mo(VI) exists as the MoO_4^{2-} anion and electrostatic interactions with surface sites become less important (Smedley and Kinniburgh, 2017). However, MoO_4^{2-} is readily adsorbed onto Fe-(hydr)oxides, pyrite, and organic matter below pH 6-7 (Bostick

et al., 2003; Goldberg and Forster, 1998; Gustafsson and Tiberg, 2015). Precipitation of relatively insoluble metal molybdates (e.g., $CaMoO_4$, $PbMoO_4$, and $NiMoO_4$) has been reported in neutral to alkaline mine tailings due to elevated ionic activities in those environments (Blanchard et al., 2015; Conlan et al., 2012; Essilfie-Dughan et al., 2011). Thiomolybdates can be prominent aqueous Mo species in sulfidic environments ($[\Sigma H_2S_{(aq)}] > 11$ μM) and are more reactive than MoO_4^{2-} (Smedley and Kinniburgh, 2017). Molybdenum(IV) is added directly to a hydroconversion process prior to coking in the form of MoS_2 catalyst pellets supported by γ-Al_2O_3 (Gray, 2015) and is thus a potential source for Mo in fluid petroleum coke and associated leachates.

Molybdenum is a common contaminant in mine-affected waters, yet a lack of scientific studies on Mo geochemistry in these settings has been highlighted as an environmental issue (Frascoli and Hudson-Edwards, 2018). More specifically, controls on Mo mobility in petroleum coke deposits are largely unknown. Understanding the geochemical processes that influence Mo mobility from petroleum coke will help to identify the long-term environmental risk posed by these deposits and will assist reclamation efforts both for these sites and for other mine-affected sites in general. The objectives of this study are to (i) determine the speciation and coordination chemistry of Mo in coke solids, (ii) identify the geochemical mechanisms controlling Mo mobility in pore water, and (iii) develop a conceptual model for Mo geochemistry of fluid petroleum coke deposits.

2. Site description

Fluid coke samples were collected from petroleum coke deposits at the Mildred Lake mine, located approximately 35 km north of Fort McMurray, Alberta, Canada. Fluid petroleum coke is generated during the bitumen upgrading process and is produced from the non-distillable bitumen fraction. This fraction is cycled between a burner and a coking vessel between 480 and 565 °C to

thermally convert long-chain hydrocarbons to volatile short-chain hydrocarbons. The remaining coke material is transported as a slurry with OSPW, which is slightly alkaline and contains elevated Na concentrations, to subaerial deposits.

Three distinct coke deposits were sampled (Fig. 1) as described by Nesbitt et al. (2017). Coke beach (CB) and coke watershed (CW) are located within the western margin of the Mildred Lake settling basin (MLSB) containment dyke. Coke beach is an uncovered 1.5 km^2 deposit and runs along the west boundary of the MLSB. Deposition of coke at CB has continued since 2000. Coke watershed is a 0.28 km^2 inactive deposit (since 2003) covered with a reclamation cover and is located along the southwestern corner of CB. These two deposits are hydraulically connected to the MLSB, which contains OSPW and fluid fine tailings from the bitumen extraction process. The water table is situated between 0.6 and 1.6 m below the surface at CB sample locations and 2.9 to 4.5 m below the surface at CW sample locations. Coke cell 5 (CC5) is a separate inactive deposit (since 1999) with an established reclamation cover spanning 0.90 km^2. All CC5 samples were positioned above the water table. Samples from four locations from CB (sites A, AM, AB, and AX), one location from CW (site CX), and one location from CC5 (site DM) were selected for this study.

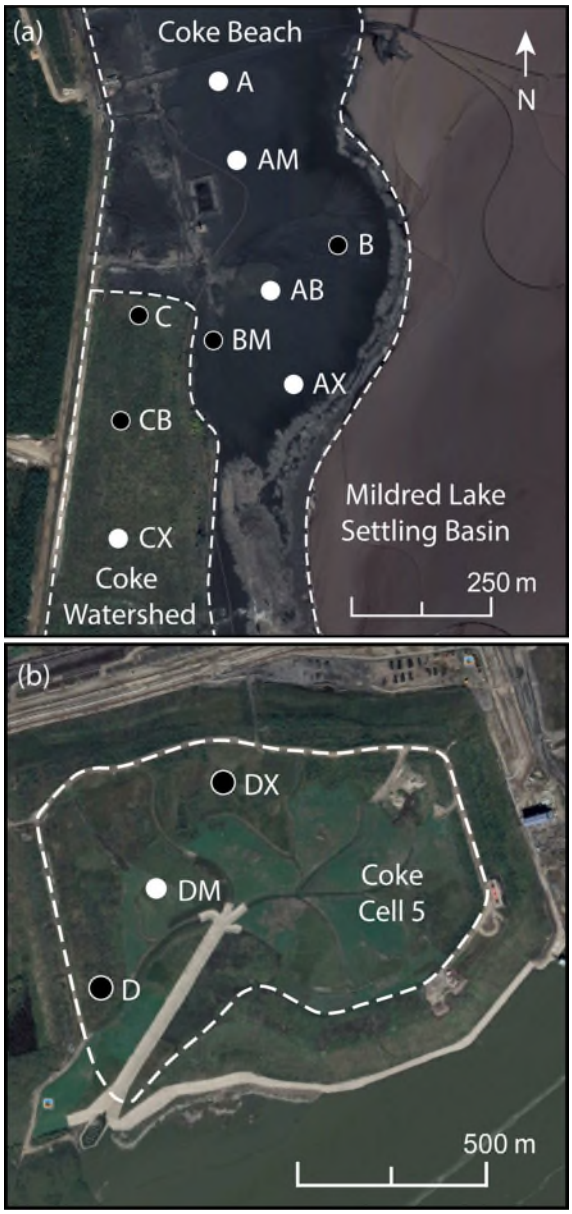

Figure 1. Satellite views and sampling locations for a) coke beach (CB) and coke watershed (CW) and (b) coke cell 5 (CC5). Locations of samples that were analyzed in this study are indicated by white circles. Satellite images attributed to Google™ Earth © 2018 Digital Globe.

3. Materials and methods

3.1 Pore water sampling and analyses

Sampling procedures are detailed by Nesbitt (2016) and Nesbitt and Lindsay (2017). Briefly, multilevel groundwater wells constructed of 0.3 cm inner diameter polyethylene tubing

were installed at multiple sites at the Mildred Lake mine site (Fig. 1). A bundle of tubing with various individual tube lengths and a 1.9 cm ID PE central standpipe was inserted into a steel drill casing spanning 6.0 to 8.0 m below the surface at each well location. The bottom 10 cm of each tube in the bundle were perforated and fitted with 125 μm Nitex mesh filters. After at least 30 days, the static water table elevation was measured in the well's central standpipe and three well volumes were purged from each well using a peristaltic pump. The well tubing was connected to platinum-cured silicon tubing attached to a sealed flow-through cell equipped with a pH electrode (Orion 8156BNUWP ROSS Ultra, Thermo Scientific), oxidation-reduction potential (ORP) electrode (Orion 9678BNWP, Thermo Scientific), and conductivity cell (Orion 013010MD, Thermo Scientific). ZoBell's and Light's solution were used to confirm the performance of the ORP electrode. The ORP measurement was temperature-corrected and adjusted relative to the standard hydrogen electrode (Eh). The flow-through cell was disconnected after the measurements were collected and field measurements of alkalinity and $H_2S_{(aq)}$ were made on pore water samples passed through 0.45 μm polyethersulfone filters. Alkalinity was measured by titrating with H_2SO_4 to the bromocresol green methyl red end point, while $H_2S_{(aq)}$ was measured using the methylene blue method. Pore water samples were filtered through 0.45 μm surfactant-free cellulose acetate filters and stored in polyethylene bottles at 4°C. Samples to be measured for trace elements were filtered through 0.1 μm polyethersulfone syringe filters, acidified to <pH 2 using concentrated trace metal grade nitric acid, and stored in PE bottles at 4 °C. A NexION 300D (PerkinElmer) inductively coupled plasma mass spectrometer (ICP-MS) was used to measure trace elements in the pore water.

Geochemical modeling was performed using PHREEQCi (v.3.3.11.12535; Parkhurst and Appelo, 2013) to calculate the aqueous speciation of Mo and saturation state of Mo-bearing

minerals in the coke pore waters. Chemistry of pore water samples (i.e., pH, Eh, alkalinity, anions, cations, and trace elements) was used as the model input. The MINTEQ.V4 thermodynamic database was used for model calculations.

3.2 Petroleum coke sampling and analyses

Continuous core samples were collected alongside the multilevel groundwater wells previously described (Fig. 1). An amphibious track-mounted sonic drill rig was used to extract cores to a depth of 8 m below the surface. The cores were sub-sampled at 0.5 m intervals. The sub-samples were sealed in high-density polyethylene bottles, transported on ice to the University of Saskatchewan, and stored at -18 °C until analysis. Samples were thawed, vacuum filtered, and prepared in an anoxic chamber (95 vol % N_2, 5 vol % H_2). Samples from select locations and depth were analyzed for bulk elemental composition. A modified aqua regia digest (1:1:1 HNO_3-HCl-deionized H_2O, at 80 °C for 1 h) was used to dissolve the coke samples and measure Mo concentrations by ICP-MS (Table 1). Two fluid coke samples were also obtained: a fresh, dry coke sample (DC), and a fresh coke sample slurried with OSPW (SC). Field samples were labelled with their site location and depth below the surface (in cm).

Table 1. Characteristics of petroleum coke samples. Molybdenum concentrations were measured using a modified aqua-regia digest followed by ICP-MS.

Sample	Depth Below Surface (m)	Depth Below Water Table (m)	Mo (mg kg^{-1})	pH Point of Zero Charge
A000	0.0	-1.1	18.4	5.7
A200	2.1	0.9	11.8	6.1
A600	5.9	4.9	22.4	6.8
AB000	0.0	-1.6	10.1	
AB200	2.0	0.4	15.9	
AB700	7.0	5.4	14.6	
AM200	2.0	1.4	19.0	6.4
AM350	3.5	2.9	15.4	
AM650	6.5	5.9	10.0	
CX050	0.5	-2.6	11.3	7.0
CX300	3.0	-0.1	9.6	6.5
CX500	5.0	1.9	11.7	5.3
DM050	0.5	N/A[a]	13.7	5.1
DM550	5.5	N/A[a]	10.7	
DM950	9.5	N/A[a]	11.8	
DC	N/A[b]	N/A[b]	N/A[b]	6.6
SC	N/A[b]	N/A[b]	N/A[b]	7.1
Average			13.8±3.8	6.3±0.7

[a] The water table was below all samples collected at site DM and was not measured.

[b] Samples DC and SC were fresh coke samples obtained prior to deposition. Compositional data were not collected for these samples.

3.3 pH point of zero charge

The pH point of zero charge (pH_{pzc}) of fluid petroleum coke was measured using a combination of the methods used by Pourrezaei et al. (2014) and Alam et al. (2016). Two separate sodium chloride (NaCl) solutions were measured (0.01 M and 0.1 M) to test the effect of background electrolyte concentration on the pH_{pzc}. Both NaCl solutions were purged with $N_{2(g)}$ for 48 h to remove dissolved CO_2 (Alam et al., 2016). For each sample, nine 40 mL amber glass vials

were filled with 25 mL of N_2-purged 0.1 M or 0.01 M NaCl solution in an anoxic chamber (≤ 5 vol. % $H_{2(g)}$, balance $N_{2(g)}$). The solution pH in each vial was adjusted to between pH 2 and 10 at pH intervals of approximately one pH unit (i.e., 2, 3, 4, 5, 6, 7, 8, 9, 10) using 0.1 N hydrochloric acid (HCl) or sodium hydroxide (NaOH). After the initial pH of each vial stabilized, the pH value was recorded and 0.5 g of gently-ground, homogenized, and vacuum-filtered coke was added to each vial. The vials were sealed in the anoxic chamber using gas-impermeable rubber-lined septa. The vials were shaken for 48 hours at 60 RPM. The change in pH after 48 hours was plotted against the initial pH and the pH_{pzc} was determined to be the pH where $pH_{initial} = pH_{final}$ (Alam et al., 2016; Pourrezaei et al., 2014).

3.3 X-ray absorption spectroscopy

Select samples were analyzed via Mo K-edge X-ray absorption near edge structure (XANES) and extended X-ray absorption fine structure (EXAFS) spectroscopy. Vacuum-filtered and vacuum-desiccated coke samples were ground using an agate mortar and pestle. The powdered coke was packed in 1.5 mm thick Teflon sample holders and sealed under anoxic conditions using three layers of Kapton tape. The samples were transported to the Canadian Light Source (CLS) in a vacuum-sealed container.

Molybdenum K-edge X-ray absorption spectroscopy (XAS) was performed at the HXMA beamline (06ID-1) at the CLS. A Si(220) double-crystal monochromator was used to select incident X-ray energy and Pt-mirrors were used to focus the X-ray beam. The monochromator was detuned to 50% flux to reject higher-order harmonics. Fluorescence data were collected using a 32-element Ge detector. A Zr-filter and Soller slits were placed between the sample and detector to enhance signal-to-noise ratios. The transmission spectrum of a downstream Mo-foil was collected simultaneously for energy calibration. Scans were performed under ambient conditions

and at least four scans per sample were collected. Each scan ranged from -200 eV below the Mo K-edge (20,000 eV) to k = 14 $Å^{-1}$. Data were collected at 0.25 eV steps in the XANES region and 0.05 $Å^{-1}$ steps in the EXAFS region.

Data reduction and analyses were performed using the XAS data analysis programs ATHENA and ARTEMIS (Demeter v.0.9.25; Ravel and Newville, 2005). Linear combination fitting (LCF) of the XANES region was performed using reference spectra for MoS_2, MoO_2, MoO_3, $NiMoO_4$, $FeMoO_4$, $CaMoO_4$, Mo(VI)-adsorbed ferrihydrite, and Mo(VI)-adsorbed goethite (Das et al., 2016; Essilfie-Dughan et al., 2011). Principal component analysis (PCA) and target transformations of the XANES region were used to estimate the number of components present in the dataset and the reference compounds that best describe the samples. Non-linear least-squares fitting of Mo K-edge EXAFS was performed to evaluate the local coordination environment of solid-phase Mo in coke samples. Amplitude and phase functions calculated from the structures of molybdenite and $Fe_2(MoO_4)_3$ using FEFF 6.0 were used to fit Mo-O, Mo-S, and Mo-Mo scattering paths. The fitting routine was performed on the Fourier transform of the background-subtracted k^3-weighted $\chi(k)$ spectrum from k = 3.0–12.0 $Å^{-1}$.

4. Results and discussion

4.1 Aqueous geochemistry

Pore water Mo concentrations in CB and CW deposits increased with depth over the upper 2 to 3 m below the water table from 0.14 mg L^{-1} to a maximum concentration of 2.2 mg L^{-1} (Fig. 2). At depths greater than 3 m, pore water Mo concentrations were relatively constant, averaging approximately 1 mg L^{-1}. Geochemical modeling indicated MoO_4^{2-} was the dominant aqueous Mo species for all sampling locations and depths. The pH of the coke pore water increased with depth,

with the top of the saturated zone being slightly acidic to neutral (pH 6 to 7.5) and lower depths transitioning to slightly alkaline conditions (pH 7.5 to 8.5; Fig. 2). Conversely, the Eh of the coke pore water decreased with depth, transitioning from oxic to anoxic conditions (Fig. S1). Infiltration of meteoric water contributes to the slightly acidic and oxic conditions in the upper 1 to 2 m of the saturated zone, while the increase in pH with depth occurs due to mixing with alkaline, anoxic OSPW originating from the adjacent Mildred Lake settling basin (Nesbitt and Lindsay, 2017). The generalized mixing zone of these two water sources occurs between 2 to 4 m below the water table and is signified by the increasing electrical conductivity (EC; Fig. 2) as the contribution of OSPW increases.

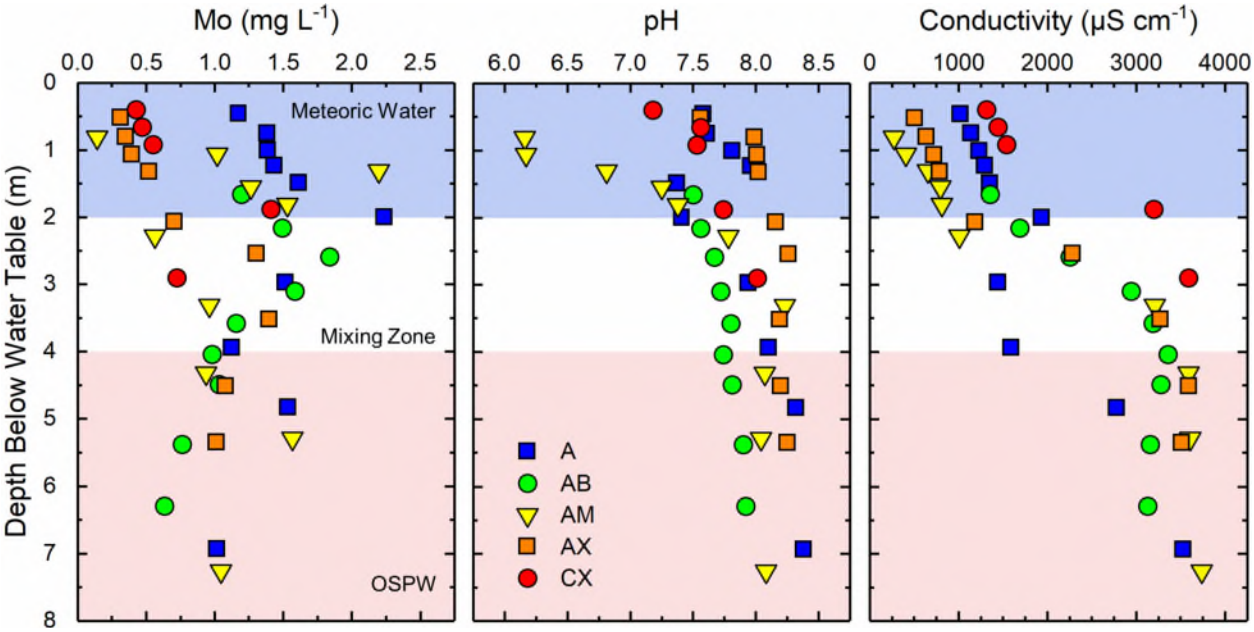

Figure 2. Depth profiles of Mo, pH, and electrical conductivity in coke pore waters.

Increasing Mo concentrations generally coincided with the water composition transitioning from meteoric water to OSPW where pH and EC increased. At lower pH and EC, Mo concentrations were generally at a minimum; the lowest Mo concentration (0.14 mg L^{-1}) occurred at site AM near the top of the water table with pH and EC minima of 6.2 and 280 µS cm^{-1}. Within

the mixing zone, Mo concentrations increased to between 1.4 to 2.2 mg L^{-1}. At multiple sites, Mo and EC increased simultaneously in the first 3 m. Past studies demonstrate Mo is readily leached from coke in both deionized water and solutions with elevated salt contents (Kessler and Hendry, 2006; Puttaswamy and Liber, 2012). Additionally, the presence of HCO_3^- and Cl^- increases Mo mobilization from coke relative to deionized water (Puttaswamy and Liber, 2012), and agrees with the observation of increased pH and EC enhancing Mo mobility in the coke deposits.

The pH_{pzc} of a surface strongly influences the mobility of outer-sphere adsorption complexes. The average pH_{pzc} for fluid petroleum coke samples was determined to be 6.3±0.7 (Table 1 and Fig. S2). This value is in agreement with previous measurements from Nesbitt et al. (2018) and Pourrezaei et al. (2014), but is greater than the value of 2.5 reported by Alam et al (2016). The range of measured pH_{pzc} values was 5.1 to 7.1 and is explained by the heterogeneous nature of coke; quartz, aluminosilicate, Fe-oxide, Ti-oxide, and pyrite contents in coke vary (Nesbitt et al., 2017) and likely influence the bulk pH_{pzc} (Sposito, 1998). In almost all cases, the pore water pH was above the bulk pH_{pzc}, suggesting that the bulk coke surface is net-neutral or negatively charged in the saturated zone and is unfavourable for MoO_4^{2-} attenuation via outer-sphere complexation. Phases within coke that can potentially adsorb MoO_4^{2-} include Fe-(hydr)oxides, pyrite, clays, and organic matter which typically adsorb MoO_4^{2-} strongest under mildly acidic conditions (~pH 3-6) (Bostick et al., 2003; Goldberg et al., 1996; Gustafsson and Tiberg, 2015; Nesbitt et al., 2017; Xu et al., 2006). Conversely, adsorption capacities of these phases decrease with increasing pH and ionic strength, with minimal adsorption occurring above pH 8 (Goldberg and Forster, 1998; Gustafsson and Tiberg, 2015). The sensitivity of aqueous Mo concentrations to pH and EC is indicative of outer-sphere MoO_4^{2-} adsorption complexes with mineral surfaces in fluid petroleum coke.

Pore water was generally undersaturated with respect to metal molybdates, although $NiMoO_4$ and $CaMoO_4$ approached saturation at many depths (Fig. S1). Molybdates may precipitate in zones where Mo concentrations are at a maximum, such as in the mixing zones at sites A and AM (Fig. 2). However, saturation indices throughout the coke deposits indicate that precipitated molybdates should dissolve. Molybdenite (MoS_2) was saturated in zones with elevated concentrations of $H_2S_{(aq)}$, but it is not expected to precipitate under ambient temperature and pressure conditions (Smedley and Kinniburgh, 2017).

4.2 Solid-phase Mo speciation

The XANES region (i.e., -200 to +50 eV relative to the Mo K-edge) of the XAS data was used to determine the oxidation state of Mo and identify the major solid-phase Mo species in the coke samples. Molybdenum(VI) compounds exhibit a distinct pre-edge feature at 20,006 eV and maximum absorbance around 20,038 to 20,042 eV (Fig. 3a), which is dependent on the Mo(VI) coordination environment (Wagner et al., 2017). Spectra of Mo(IV) compounds do not contain a pre-edge and the maximum absorbance occurs at lower energies (~20,030 eV).

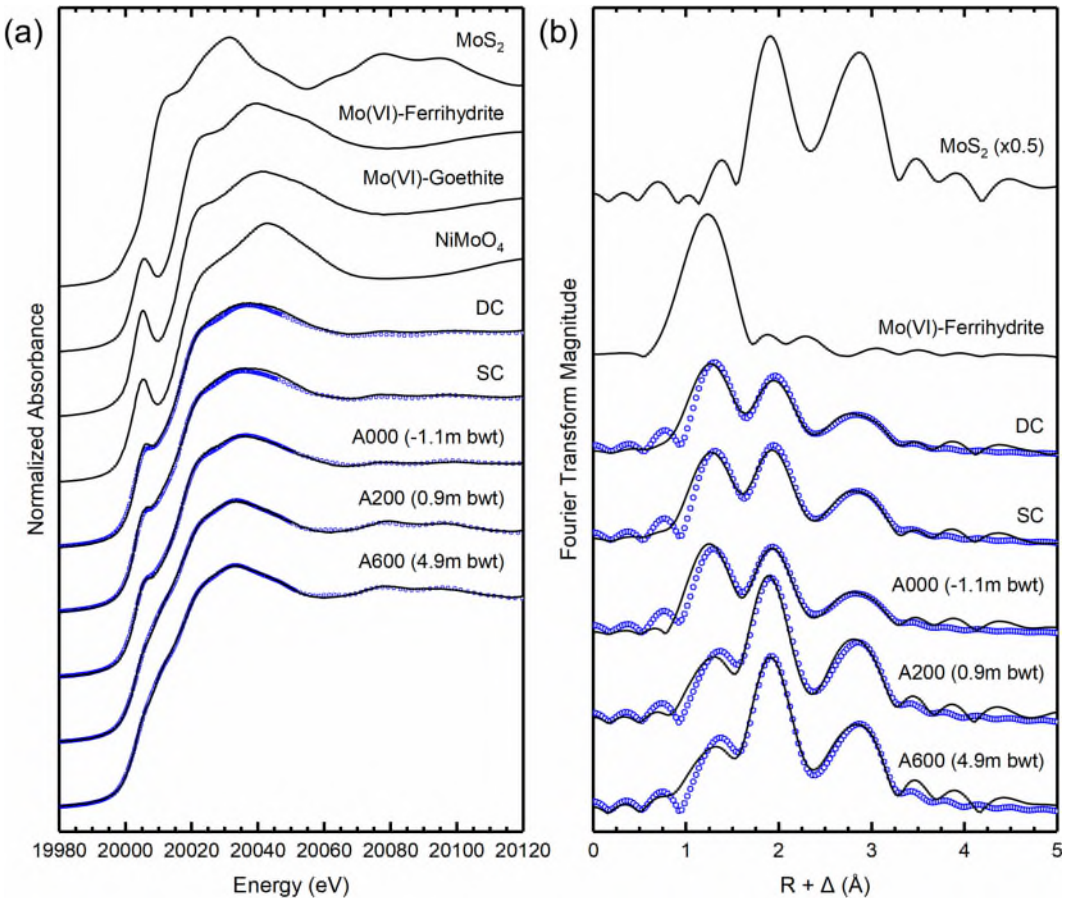

Figure 3. (a) X-ray absorption near edge spectra and (b) Fourier transforms of the k^3-weighted $\chi(k)$ spectra of select samples and standard compounds for the Mo K-edge. Solid lines represent measured data and open circles represent linear combination fits (XANES) non-linear least squares fits (Fourier transforms). Numbers in parentheses are the sample depths (m) below the water table (bwt).

The pre-edge intensity and white line positions for fresh, dry coke (DC) indicate Mo(VI) dominates, although the decreased pre-edge intensity and lower-energy maximum absorbance relative to a Mo(VI) standard suggest the presence of Mo(IV) in the sample as well (Fig. 3a). Spectra obtained for slurried coke (SC) and the surface coke layer were similar and slightly reduced relative to DC. Samples collected from below the water table of the coke deposits exhibit increasingly similar characteristics to Mo(IV) with little to no pre-edge peak and a maximum absorbance occurring at a lower energy. This observation suggests that the proportion of solid-

phase Mo(VI) decreases with depth. A similar trend with depth was observed at all sample locations (Fig. S3).

A combination of Mo(VI) and Mo(IV) reference compounds were used for LCF analysis. The reference compounds chosen for the final LCF results were based on fit quality, pore water analysis, previous geochemical characterization of coke from the study site, geochemical modeling, and PCA. Pore water chemistry suggested the presence of MoO_4^{2-} adsorption complexes was probable. Nesbitt et al. (2017) identified Fe-oxides and pyrite in the same set of coke samples and supports the possibility of Mo(VI) surface complexation. Molybdate adsorbed on ferrihydrite and goethite were used as reference compounds and coordination environment analogues for outer-sphere and inner-sphere Mo(VI) surface complexes, respectively (Das et al., 2016). Molybdenum(IV) disulfide was included in all fits because a MoS_2 catalyst is added in the coking process. Nickel molybdate fit well in many samples; however, the pore water data indicated that $NiMoO_4$ was undersaturated in the coke deposits and suggests it is likely not present in the samples. Principal component analysis (Fig. S4) indicated that three reference compounds could be used to describe the data set. Target transformations (Fig. S5) suggested that MoS_2 and MoO_4^{2-} adsorbed to ferrihydrite and goethite were the most likely candidates of the set of reference compounds used.

The LCF results for DC showed a predominance of Mo(VI) in the form of inner- and outer-sphere MoO_4^{2-} complexes (modeled as MoO_4^{2-} adsorbed to goethite and ferrihydrite, respectively) while the remaining Mo was Mo(IV) in the form of MoS_2 (Fig. 4a and Table S1). The amount of outer-sphere MoO_4^{2-} in fresh coke decreased after being contacted with mildly alkaline OSPW (sample SC). In coke samples above the water table, outer-sphere MoO_4^{2-} surface complexes were the predominant Mo species, with inner-sphere MoO_4^{2-} surface complexes and MoS_2 making up

the balance (Fig. 4b). In coke samples collected from below the water table (Fig. 4c), the average Mo oxidation state and the amount of outer-sphere MoO_4^{2-} decreased sharply. The degree of inner-sphere surface complexation, however, remained relatively constant across the water table and with depth. These trends agree with the previous discussion on the bulk pH_{pzc} of the coke samples; the increasing pH and EC of the pore water with depth increases the negative charge density of surface sites and readily mobilizes outer-sphere MoO_4^{2-} to the coke pore water. Samples from CC5 were all above the water table. Outer-sphere MoO_4^{2-} complexes were not observed in the two samples at lower depths, suggesting the outer-sphere complexes have been mobilized (Fig. 4d).

Molybdenum(IV) disulfide, which originates from the addition of MoS_2 catalyst in the process, generally increased with depth. This apparent increase of MoS_2 is likely due to the actual decrease of MoO_4^{2-} surface complexes. Although HS^- is present in the pore water, secondary MoS_2 (jordisite or molybdenite) precipitation is unlikely as the elevated temperatures and pressures required for precipitation of these phases (Smedley and Kinniburgh, 2017) do not occur in the coke deposits. Oxidation of MoS_2 by infiltrating meteoric water in the unsaturated zone is possible and could be a potential source of mobile Mo; however, MoS_2 is resistant to oxidative weathering relative to other sulfides and leaching would be kinetically limited (Lindsay et al., 2015).

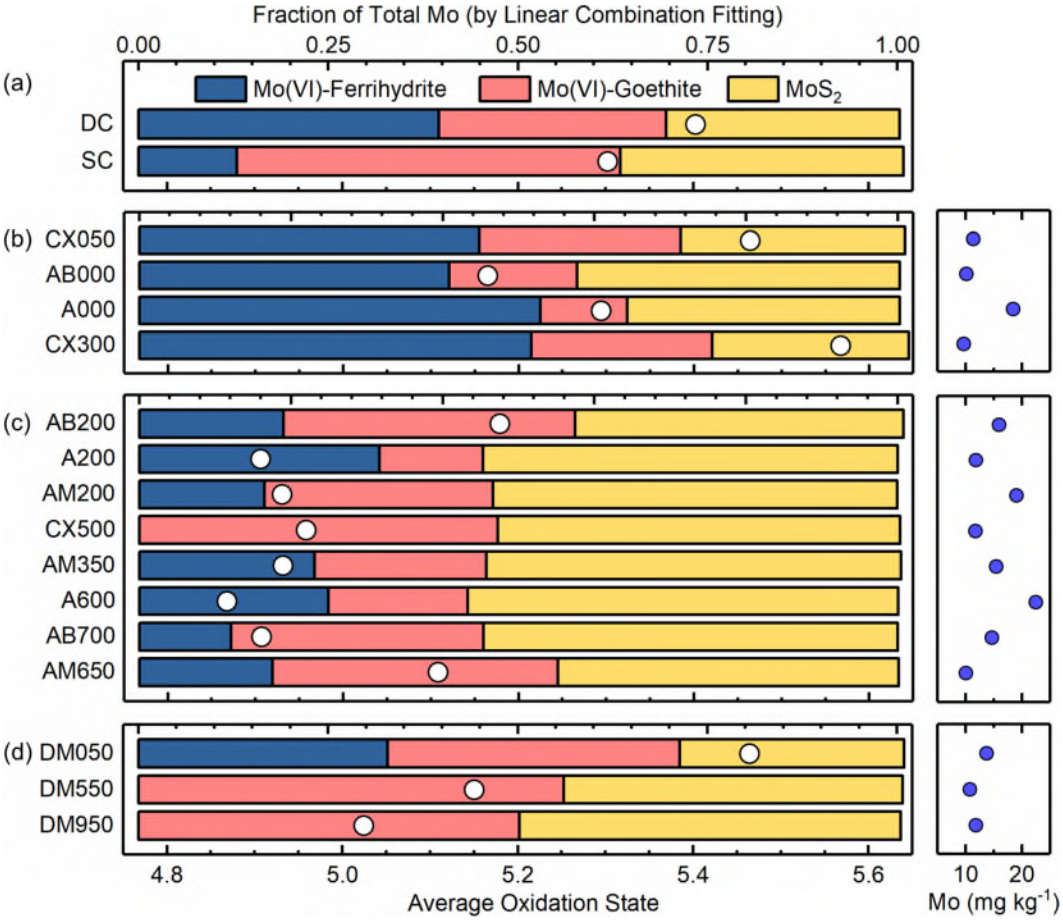

Figure 4. Linear combination fit results and solid-phase Mo concentrations of (a) fresh coke samples, (b) unsaturated zone CB and CW samples, (c) saturated zone CB and CW samples, and (d) coke cell 5 samples. Samples are sorted by increasing depth relative to the water table. Coloured bars represent LCF results and white circles denote the average oxidation state of the sample calculated from LCF results.

4.3 Local coordination environment of molybdenum

Three distinct types of backscatterers were evident in the Fourier transformed EXAFS data: (i) a Mo-O shell at an interatomic distance of ~1.75 Å; (ii) a Mo-S shell at ~2.41 Å; and (iii) a Mo-Mo shell at ~3.17 Å (Table 2, Fig. 3b and Fig. S6). The Mo-O shell is indicative of Mo(VI) tetrahedrally coordinated with O at a distance of 1.75 to 1.77 Å (Arai, 2010; Das et al., 2016) and is attributed to both outer- and inner-sphere MoO_4^{2-} surface complexes. The combination of the Mo-S and Mo-Mo shells suggest the presence of Mo(IV) as a MoS_2-type phase. Structural models

were developed for each coke sample using these three shells. A multiple scattering path representing a scattered photoelectron in the molybdate tetrahedron was included for each model and improved the fits for all samples.

The interatomic distances of each coordination shell for all samples ranged from 1.74 to 1.75 Å (Mo-O), 2.40 to 2.41 Å (Mo-S), and 3.16 to 3.17 Å (Mo-Mo). This finding indicates that the general coordination environment did not noticeably vary between samples (Table 2). However, the coordination number of each shell varied and indicated the relative proportions of each Mo phase changed in each sample, suggesting potential mechanisms for Mo mobility. The Mo-O coordination numbers of samples above the water table (1.5 - 2.1) were approximately equal to those in DC and SC. Conversely, the Mo-O coordination numbers of samples below the water table (1.1 - 1.6) were less than those in DC and SC, while the coordination number of Mo-S and Mo-Mo shells increased below the water table. These trends indicate there is less adsorbed MoO_4^{2-} below the water table as it is mobilized to the pore water.

The fitting results of the samples show an average of 1.5 times more Mo-S bonds compared to Mo-Mo neighbours. This coordination environment is consistent with the small MoS_2 crystallites deposited on a support material in the added MoS_2 catalyst (Gray, 2015; Miller et al., 2001, 2000). As such, Mo(IV) in the fluid petroleum coke is likely derived from entrained particles of the MoS_2 catalyst.

Table 2. Fitting parameters for Mo K-edge EXAFS fitting results of all petroleum coke samples.

		Mo-O Shell			Mo-S Shell			Mo-Mo Shell			
	ΔE_0 (eV)	**CN**	**R (Å)**	**σ^2 (Å^2)**	**CN**	**R (Å)**	**σ^2 (Å^2)**	**CN**	**R (Å)**	**σ^2 (Å^2)**	**R-factor**
AB000	-5 (1)	1.6 (1)	1.746 (6)	0.002	2.6 (1)	2.407 (8)	0.003	1.7 (2)	3.166 (8)	0.003	0.010
AB200[a]	-4 (1)	1.5 (1)	1.748 (5)	0.002	2.5 (1)	2.411 (7)	0.003	1.6 (2)	3.172 (7)	0.003	0.009
AB700[a]	-4.1 (8)	1.1 (1)	1.744 (6)	0.002	3.3 (1)	2.412 (5)	0.003	2.2 (2)	3.173 (6)	0.003	0.006
CX050	-4 (2)	1.9 (2)	1.74 (2)	0.003	1.5 (2)	2.40 (2)	0.004	0.9 (2)	3.16 (2)	0.004	0.030
CX300	-5 (2)	2.1 (2)	1.744 (9)	0.003	1.6 (1)	2.40 (1)	0.004	1.1 (2)	3.16 (2)	0.004	0.020
CX500[a]	-5.6 (8)	1.6 (1)	1.751 (4)	0.003	3.1 (1)	2.406 (5)	0.003	1.9 (1)	3.169 (5)	0.003	0.005
DM050	-7 (2)	1.9 (1)	1.750 (8)	0.003	1.8 (1)	2.41 (1)	0.004	1.1 (2)	3.17 (1)	0.004	0.018
DM550	-7 (1)	1.8 (1)	1.753 (5)	0.003	2.8 (1)	2.408 (6)	0.003	2.0 (2)	3.172 (7)	0.003	0.007
DM950	-5.6 (8)	1.5 (1)	1.748 (4)	0.003	3.0 (1)	2.407 (4)	0.003	2.0 (1)	3.165 (4)	0.003	0.005
A000	-4 (2)	1.8 (1)	1.740 (7)	0.003	1.9 (1)	2.397 (9)	0.003	1.1 (2)	3.16 (1)	0.003	0.014
A200[a]	-3 (1)	1.4 (2)	1.743 (9)	0.003	3.5 (2)	2.402 (8)	0.004	2.4 (3)	3.168 (9)	0.004	0.014
A600[a]	-3 (1)	1.4 (1)	1.745 (7)	0.003	3.7 (1)	2.410 (6)	0.004	2.6 (2)	3.171 (6)	0.004	0.008
AM200[a]	-3 (1)	1.4 (1)	1.744 (7)	0.003	3.1 (1)	2.407 (6)	0.003	2.0 (2)	3.170 (7)	0.003	0.010
AM350[a]	-2 (1)	1.1 (1)	1.738 (7)	0.002	3.0 (1)	2.410 (5)	0.003	1.9 (2)	3.174 (6)	0.003	0.007
AM650[a]	-4 (1)	1.6 (1)	1.747 (5)	0.002	2.7 (1)	2.404 (7)	0.003	1.8 (2)	3.166 (7)	0.006	0.009
DC	-3 (1)	1.9 (1)	1.749 (5)	0.003	2.0 (1)	2.409 (7)	0.004	1.2 (1)	3.167 (8)	0.004	0.007
SC	-3 (1)	1.7 (1)	1.751 (5)	0.002	2.2 (1)	2.410 (7)	0.003	1.4 (1)	3.171 (7)	0.003	0.007

[a] Sample was collected below the water table.

[b] ΔE_0 = energy shift. CN = coordination number. R = interatomic distance. σ^2 = Debye-Waller factor, constrained in all fits to minimize variables. A multiple scattering shell (Mo-O-O) was fit for all samples and was constrained to CN = $3CN_{Mo\text{-}O}$, $\sigma^2 = 2\sigma^2_{Mo\text{-}O}$, R = 3.16 Å. The amplitude reduction factor, S_0^2, was fixed at 0.9 for all samples. The fitting ranges used were k = 3.0 - 12.0 Å^{-1} and R = 1.0 - 3.3 Å.

Additional model configurations were fit to the data to test for extended shells predicted in the LCF analysis. To model inner-sphere MoO_4^{2-} complexes with Fe-(hydr)oxides, shells representing edge-sharing and corner-sharing coordination at ~2.8 Å and ~3.5 Å were added to the model (Arai, 2010; Das et al., 2016). The fit quality when a corner-sharing complex was included was comparable to the final fits; however, the resulting coordination number of the complex ranged from 0.1 to 0.3 in most samples, and was deemed insignificant. Octahedral MoO_6 geometries, which can form with goethite and organic matter (Arai, 2010; Wichard et al., 2009), consistently

returned poor fits and were, therefore, ruled out of consideration. Nickel shells were also considered as Ni is often added to the structure of MoS_2 catalysts (Gray, 2015) but all models with Ni shells returned insignificant Mo-Ni coordination numbers.

Due to the organic-rich nature of petroleum coke, organic-associated Mo was also considered. Carboxylate groups in natural organic matter can adsorb Mo(VI) in an octahedral coordination geometry (Wichard et al., 2009). Gradual desorption of Mo(VI) from natural organic matter occurs above pH 6 (Gustafsson and Tiberg, 2015), and could be a source of mobile Mo in coke below the water table. However, the lack of octahedral Mo in the EXAFS data suggests octahedral Mo(VI)-organic complexes are minor or absent. The chemical complexity of these samples likely precludes the identification of minor components that could be present in the second shell fits attempted here.

5. Conceptual model for Mo geochemistry

Molybdenum occurs in fluid petroleum coke as both Mo(IV) and Mo(VI), with the latter species being the most mobile under the geochemical conditions of the coke deposits. Tetrahedral molybdate (MoO_4^{2-}) is the major (>50%) Mo species in fresh coke and is likely associated with mineral surfaces in both inner- and outer-sphere arrangements. Molybdenum(IV) disulfide catalyst particles added during bitumen upgrading are likely the main source of reduced Mo in the fresh coke.

The unsaturated layer of the coke deposits is infiltrated by oxic and mildly acidic meteoric water. While MoS_2 may be oxidized in this layer, MoS_2 is strongly resistant to oxidation (Lindsay et al., 2015; Plumlee, 1999) and is likely only a source of soluble Mo in the long-term. Due to the

slightly acidic pH of meteoric water, Mo(VI) adsorption complexes should be mostly stable in the unsaturated zone, although slow leaching of Mo is still possible.

In the saturated zone, the pH and EC of the pore water increase with depth as the pore water mixes with alkaline and Na-rich OSPW infiltrating from the adjacent Mildred Lake settling basin. These conditions mobilize outer-sphere MoO_4^{2-} surface complexes in the mixing zone between meteoric water and OSPW and increase aqueous Mo concentrations in this region. This is likely the main mechanism of Mo leaching to the coke pore water. Metal molybdates, such as $NiMoO_4$ and $CaMoO_4$ are slightly undersaturated in the coke pore water and are likely to dissolve if they are present in the coke deposits. Molybdenum(IV) disulfide is expected to remain stably bound in coke solids in the saturated zone at lower depths due to the anoxic conditions.

Acknowledgments

Funding was provided by the Natural Sciences and Engineering Research Council of Canada (NSERC) and Syncrude Canada Ltd. through the NSERC Industrial Research Chairs program (Grant No. IRCPJ-450684-13). A portion of the research described in this paper was performed at the Canadian Light Source, which is supported by the Canada Foundation for Innovation, NSERC, the University of Saskatchewan, the Government of Saskatchewan, Western Economic Diversification Canada, the National Research Council Canada, and the Canadian Institutes of Health Research. Assistance from Dr. Ning Chen and Dr. Weifeng Chen at the HXMA beamline is gratefully acknowledged. We thank Dr. Joseph Essilfie-Dughan and Dr. Soumya Das for providing XAS reference compound spectra and Mojtaba Abdolahnezhad for performing pH_{pzc} measurements on fresh coke samples (DC and SC).

Declaration of interest

Declarations of interest: none

Appendix A. Supplementary Data

Raw tables of the LCF results, XANES spectra, EXAFS spectra, PCA results, plots of pH_{pzc} measurements, and additional depth profiles are included as supplementary data.

References

AER, 2018. ST-39: Alberta Mineable Oil Sands Plant Statistics. Calgary.

Alam, M.S., Cossio, M., Robinson, L., Wang, X., Kenney, J.P.L., Konhauser, K.O., MacKenzie, M.D., Ok, Y.S., Alessi, D.S., 2016. Removal of organic acids from water using biochar and petroleum coke. Environ. Technol. Innov. 6, 141–151. doi:10.1016/j.eti.2016.08.005

Arai, Y., 2010. X-ray absorption spectroscopic investigation of molybdenum multinuclear sorption mechanism at the goethite-water interface. Environ. Sci. Technol. 44, 8491–8496. doi:10.1021/es101270g

Baker, L.F., Ciborowski, J.J.H., MacKinnon, M.D., 2012. Petroleum coke and soft tailings sediment in constructed wetlands may contribute to the uptake of trace metals by algae and aquatic invertebrates. Sci. Total Environ. 414, 177–186. doi:10.1016/j.scitotenv.2011.10.011

Blanchard, P.E.R., Hayes, J.R., Grosvenor, A.P., Rowson, J., Hughes, K., Brown, C., 2015. Investigating the geochemical model for molybdenum mineralization in the JEB tailings management facility at McClean Lake, Saskatchewan: An x-ray absorption spectroscopy study. Environ. Sci. Technol. 49, 6504–6509. doi:10.1021/acs.est.5b00528

Bostick, B.C., Fendorf, S., Helz, G.R., 2003. Differential adsorption of molybdate and tetrathiomolybdate on pyrite (FeS_2). Environ. Sci. Technol. 37, 285–291. doi:10.1021/es0257467

Caruso, J.A., Zhang, K., Schroeck, N.J., McCoy, B., McElmurry, S.P., 2015. Petroleum coke in the urban environment: A review of potential health effects. Int. J. Environ. Res. Public Health 12, 6218–6231. doi:10.3390/ijerph120606218

Conlan, M.J.W., Mayer, K.U., Blaskovich, R., Beckie, R.D., 2012. Solubility controls for molybdenum in neutral rock drainage. Geochemistry Explor. Environ. Anal. 12, 21–32. doi:10.1144/1467-7873/10-RA-043

Das, S., Essilfie-Dughan, J., Jim Hendry, M., 2016. Sequestration of molybdate during transformation of 2-line ferrihydrite under alkaline conditions. Appl. Geochemistry 73, 70–80. doi:10.1016/j.apgeochem.2016.08.003

Essilfie-Dughan, J., Pickering, I.J., Hendry, M.J., George, G.N., Kotzer, T., 2011. Molybdenum

speciation in uranium mine tailings using X-ray absorption spectroscopy. Environ. Sci. Technol. 45, 455–60. doi:10.1021/es102954b

Frascoli, F., Hudson-Edwards, K., 2018. Geochemistry, mineralogy and microbiology of molybdenum in mining-affected environments. Minerals 8, 42. doi:10.3390/min8020042

Goldberg, S., Forster, H.S., 1998. Factors affecting molybdenum adsorption by soils and minerals. Soil Sci. 163, 109–114. doi:10.1097/00010694-199802000-00004

Goldberg, S., Forster, H.S., Godfrey, C.L., 1996. Molybdenum adsorption on oxides, clay minerals, and soils. Soil Sci. Soc. Am. 60, 425–432.

Gray, M.R., 2015. Upgrading Oilsands Bitumen and Heavy Oil, 1st ed. The University of Alberta Press, Edmonton, Alberta, Canada.

Gustafsson, J.P., Tiberg, C., 2015. Molybdenum binding to soil constituents in acid soils: An XAS and modelling study. Chem. Geol. 417, 279–288. doi:10.1016/j.chemgeo.2015.10.016

Jasechko, S., Gibson, J.J., Moncur, M., Birks, S.J., Tattrie, K., Yi, Y., Eby, P., Richardson, K., 2011. Isotopic and geochemical tracers for fingerprinting process-affected waters in the oil sands industry: A pilot study. Oil Sands Research and Information Network Technical Report TR-12. doi:doi:/10.7939/R3X921J72

Kessler, S., Hendry, M.J., 2006. Geochemistry and leaching of coke from Syncrude and Suncor sites. Unpublished report. University of Saskatchewan, Saskatoon, SK.

Lindsay, M.B.J., Moncur, M.C., Bain, J.G., Jambor, J.L., Ptacek, C.J., Blowes, D.W., 2015. Geochemical and mineralogical aspects of sulfide mine tailings. Appl. Geochemistry 57, 157–177. doi:10.1016/j.apgeochem.2015.01.009

Miller, J.T., Marshall, C.L., Kropf, A.J., 2001. (Co)MoS_2/Alumina Hydrotreating Catalysts: An EXAFS Study of the Chemisorption and Partial Oxidation with O_2. J. Catal. 202, 89–99. doi:10.1006/jcat.2001.3273

Miller, J.T., Reagan, W.J., Kaduk, J.A., Marshall, C.L., Kropf, A.J., 2000. Selective hydrodesulfurization of FCC naphtha with supported MoS_2 catalysts: The role of cobalt. J. Catal. 193, 123–131. doi:10.1006/jcat.2000.2873

Nakata, C., Qualizza, C., MacKinnon, M., Renault, S., 2011. Growth and physiological responses of Triticum aestivum and Deschampsia caespitosa exposed to petroleum coke. Water. Air. Soil Pollut. 216, 59–72. doi:10.1007/s11270-010-0514-x

Nesbitt, J.A., 2016. Geochemical investigation of fluid petroleum coke deposits at an oil sand mine in northern Alberta, Canada. University of Saskatchewan.

Nesbitt, J.A., Lindsay, M.B.J., 2017. Vanadium geochemistry of oil sands fluid petroleum coke. Environ. Sci. Technol. 51, 3102–3109. doi:10.1021/acs.est.6b05682

Nesbitt, J.A., Lindsay, M.B.J., Chen, N., 2017. Geochemical characteristics of oil sands fluid petroleum coke. Appl. Geochemistry 76, 148–158. doi:10.1016/j.apgeochem.2016.11.023

Nesbitt, J.A., Robertson, J.M., Swerhone, L.A., Lindsay, M.B.J., 2018. Nickel geochemistry of oil sands fluid petroleum coke deposits, Alberta, Canada. Facets 3, 469–486. doi:10.1139/facets-2017-0115

Parkhurst, D.L., Appelo, C.A.J., 2013. Description of input and examples for PHREEQC version 3 - A computer program for speciation, batch-reaction, one-dimensional transport, and

inverse geochemical calculations, in: U.S. Geological Survey Techniques and Methods, Book 6. p. 497.

Plumlee, G.S., 1999. The environmental goelogy of mineral deposits, in: Plumlee, G.S., Logsdon, M.J. (Eds.), The Environmental Geochemistry of Mineral Deposits, Part A. Processes, Techniques, and Health Issues. Littleton, CO, pp. 71–116.

Pourrezaei, P., Alpatova, A., Chelme-Ayala, P., Perez-Estrada, L.A., Jensen-Fontaine, M., Le, X.C., Gamal El-Din, M., 2014. Impact of petroleum coke characteristics on the adsorption of the organic fractions from oil sands process-affected water. Int. J. Environ. Sci. Technol. 11, 2037–2050. doi:10.1007/s13762-013-0406-x

Puttaswamy, N., Liber, K., 2012. Influence of inorganic anions on metals release from oil sands coke and on toxicity of nickel and vanadium to Ceriodaphnia dubia. Chemosphere 86, 521–529. doi:10.1016/j.chemosphere.2011.10.018

Puttaswamy, N., Liber, K., 2011. Identifying the causes of oil sands coke leachate toxicity to aquatic invertebrates. Environ. Toxicol. Chem. 30, 2576–2585. doi:10.1002/etc.653

Puttaswamy, N., Turcotte, D., Liber, K., 2010. Variation in toxicity response of Ceriodaphnia dubia to Athabasca oil sands coke leachates. Chemosphere 80, 489–497. doi:10.1016/j.chemosphere.2010.04.071

Ravel, B., Newville, M., 2005. ATHENA, ARTEMIS, HEPHAESTUS: data analysis for X-ray absorption spectroscopy using IFEFFIT. J. Synchrotron Radiat. 12, 537–41. doi:10.1107/S0909049505012719

Shotyk, W., Bicalho, B., Cuss, C.W., Donner, M.W., Grant-Weaver, I., Haas-Neill, S., Javed, M.B., Krachler, M., Noernberg, T., Pelletier, R., Zaccone, C., 2017. Trace metals in the dissolved fraction (< 0.45 μm) of the lower Athabasca River: Analytical challenges and environmental implications. Sci. Total Environ. 580, 660–669. doi:10.1016/j.scitotenv.2016.12.012

Smedley, P.L., Kinniburgh, D.G., 2017. Molybdenum in natural waters: A review of occurrence, distributions and controls. Appl. Geochemistry 84, 387–432. doi:10.1016/j.apgeochem.2017.05.008

Sposito, G., 1998. On points of zero charge. Environ. Sci. Technol. 32, 2815–2819. doi:10.1021/es9802347

Wagner, M., Chappaz, A., Lyons, T.W., 2017. Molybdenum speciation and burial pathway in weakly sulfidic environments: Insights from XAFS. Geochim. Cosmochim. Acta 206, 18–29. doi:10.1016/j.gca.2017.02.018

WHO, 2011. WHO guidelines for drinking-water quality., Fourth. ed. WHO Press, Geneva, Switzerland. doi:10.1016/S1462-0758(00)00006-6

Wichard, T., Mishra, B., Myneni, S.C.B., Bellenger, J.-P., Kraepiel, A.M.L., 2009. Storage and bioavailability of molybdenum in soils increased by organic matter complexation. Nat. Geosci. 2, 625–629. doi:10.1038/ngeo589

Xu, N., Christodoulatos, C., Braida, W., 2006. Adsorption of molybdate and tetrathiomolybdate onto pyrite and goethite: Effect of pH and competitive anions. Chemosphere 62, 1726–1735. doi:10.1016/j.chemosphere.2005.06.025

Zhang, Y., Shotyk, W., Zaccone, C., Noernberg, T., Pelletier, R., Bicalho, B., Froese, D.G., Davies, L., Martin, J.W., 2016. Airborne petcoke dust is a major source of polycyclic aromatic hydrocarbons in the Athabasca oil sands region. Environ. Sci. Technol. 50, 1711–1720. doi:10.1021/acs.est.5b05092

Zubot, W., Mackinnon, M.D., Chelme-Ayala, P., Smith, D.W., El-Din, M.G., 2012. Petroleum coke adsorption as a water management option for oil sands process-affected water. Sci. Total Environ. 427–428, 364–372. doi:10.1016/j.scitotenv.2012.04.024